CHAPTER – 7

Crystallographic texture dependence of biocompatibility of the Ti-Zr-Nb-Mo-Fe-Cr based bio-CCA

7.1 Background

The development of implant biomaterials has increasingly focused on HEAs/CCAs in recent times due to their multifunctional properties, including excellent strength and ductility, high resistance to corrosion and wear, and favorable biocompatibility that enables seamless integration with surrounding tissues [7,12]. These properties of bio-CCAs are influenced by several factors, such as the selection of the constituent elements, processing and heat treatment conditions, microstructural characteristics, and the alloy's response to the physiological environment [112]. In this context, Chapters 5 and 6 of this thesis demonstrated that annealed $Ti_{35}Zr_{35}Nb_{15}Mo_5Fe_5Cr_5$ CCA exhibited superior mechanical properties, corrosion resistance, and biocompatibility compared to both the corresponding as-cast alloy as well as conventional biocompatible alloys. These enhanced properties in HEAs/CCAs are closely associated with microstructural changes that occur during annealing, which promote a more homogeneous microstructure [224-225].

Crystallographic texture is an integral attribute of microstructure that plays a crucial role in influencing the surface energy, corrosion resistance, and biocompatibility of alloys used in biomedical applications [226-229]. For example, specific grain orientations can demonstrate reduced corrosion rates or facilitate beneficial protein adsorption, which in turn supports improved cell adhesion and proliferation. Hoseini et al. reported that, in the case of cp-Ti, a higher number of grains oriented with <0002> planes exposed at the surface led to improved cell adhesion [229]. Similarly, Amirnejad et al. also reported that the crystallographic texture of the Ti-6Al-4V alloy affects its surface free energy [227]. An increase in surface free energy enhances surface hydrophilicity, which subsequently promotes better cell adhesion and proliferation.

Based on the aforementioned background, the aim of the present chapter is to study the underlying mechanism (specifically, crystallographic texture) that influences the biocompatibility of the $Ti_{35}Zr_{35}Nb_{15}Mo_5Fe_5Cr_5$ CCA.

7.2 Results

The in-vitro cytocompatibility of the as-cast and annealed $Ti_{35}Zr_{35}Nb_{15}Mo_5Fe_5Cr_5$ CCA specimens, including cell viability, proliferation, and adhesion of MG-63 cells, was evaluated using the MTT assay, as well as confocal and scanning electron microscopy. Figure 7.1 (a) shows the MTT assay results of the as-cast and annealed CCA samples after 3 and 7 days of incubation. The absorbance, indicative of the number of viable cells, increased noticeably from the as-cast CCA to the annealed CCA. This absorbance further increased with the extension of the incubation period from 3 to 7 days, suggesting enhanced cell proliferation.

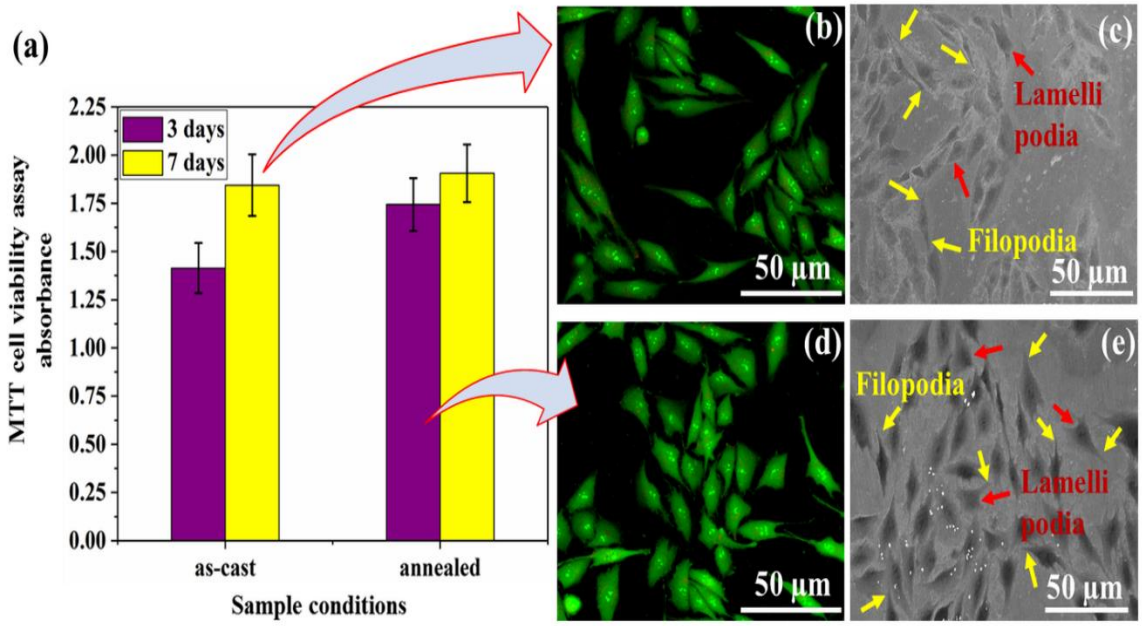

Figure 7.1 (a) MTT assay results for MG-63 cell viability and proliferation behavior after 3 and 7 days of incubation (b-e) confocal microscopy and SEM images of MG-63 cells on the surface of (b and c) as-cast CCA and (d and e) 1100ºC annealed CCA after 3 days of incubation.

The confocal microscopy images of MG-63 cells adhered on the surfaces of as-cast and annealed CCA specimens, stained with acridine orange/ethidium bromide (AO/EtBr) fluorescent dye, are shown in Figures 7.1 (b) and 1 (d). As previously discussed in Chapter 6, acridine orange stains both viable (green) and non-viable (red) cells, while ethidium bromide selectively stains cells with compromised membrane integrity, thereby indicating dead or unhealthy cells. Both the as-cast and annealed $Ti_{35}Zr_{35}Nb_{15}Mo_5Fe_5Cr_5$ CCA specimens exhibit negligible presence of dead or unhealthy cells. However, the annealed CCA shows a noticeably greater number of green-stained cells, indicating improved cell adhesion after annealing. This enhancement is likely attributed to the development of crystallographic texture during the annealing process. A similar texture-induced improvement in cell adhesion has also been reported by Hoseini et al. for cp-Ti [229].

Figures 7.1 (c and e) exhibit the SEM images of MG-63 cells adhered to and proliferating on the surfaces of as-cast and annealed $Ti_{35}Zr_{35}Nb_{15}Mo_5Fe_5Cr_5$ CCA samples after 3 days of incubation. The cells are well-spread across the surfaces, showing irregular, elongated-polygonal shapes with clearly visible filopodia and lamellipodia (indicated by yellow and red arrows), which are essential for migration and sensing of cells [121]. A greater presence of these cellular extensions (filopodia and lamellipodia) is typically associated with enhanced cell adhesion, spreading, and interaction with the material surface. Notably, the SEM image of the annealed CCA reveals a higher density of adherent MG-63 cells, along with more pronounced polygonal shapes and more prominent filopodia and lamellipodia.

These observations suggest that the annealed CCA shows superior biocompatibility compared to the as-cast state.

EBSD inverse pole figure (IPF) and image quality (IQ) maps for both the as-cast and annealed $Ti_{35}Zr_{35}Nb_{15}Mo_5Fe_5Cr_5$ CCA samples are shown in Figure 7.2. In the IPF maps, the color coding corresponds to the crystallographic orientation perpendicular to the sample surface. As shown in Figures 7.2 (a and b), the as-cast CCA exhibits a dendritic microstructure, with an average primary dendrite size of 69.94 ± 4.27 µm. In contrast, the morphology of the 1100ºC annealed CCA sample, as exhibited in Figures 2 (c and d), transforms from a dendritic structure to an irregular and approximately equiaxed grain structure. The average grain size after the annealing treatment is 29.39 ± 2.16 µm.

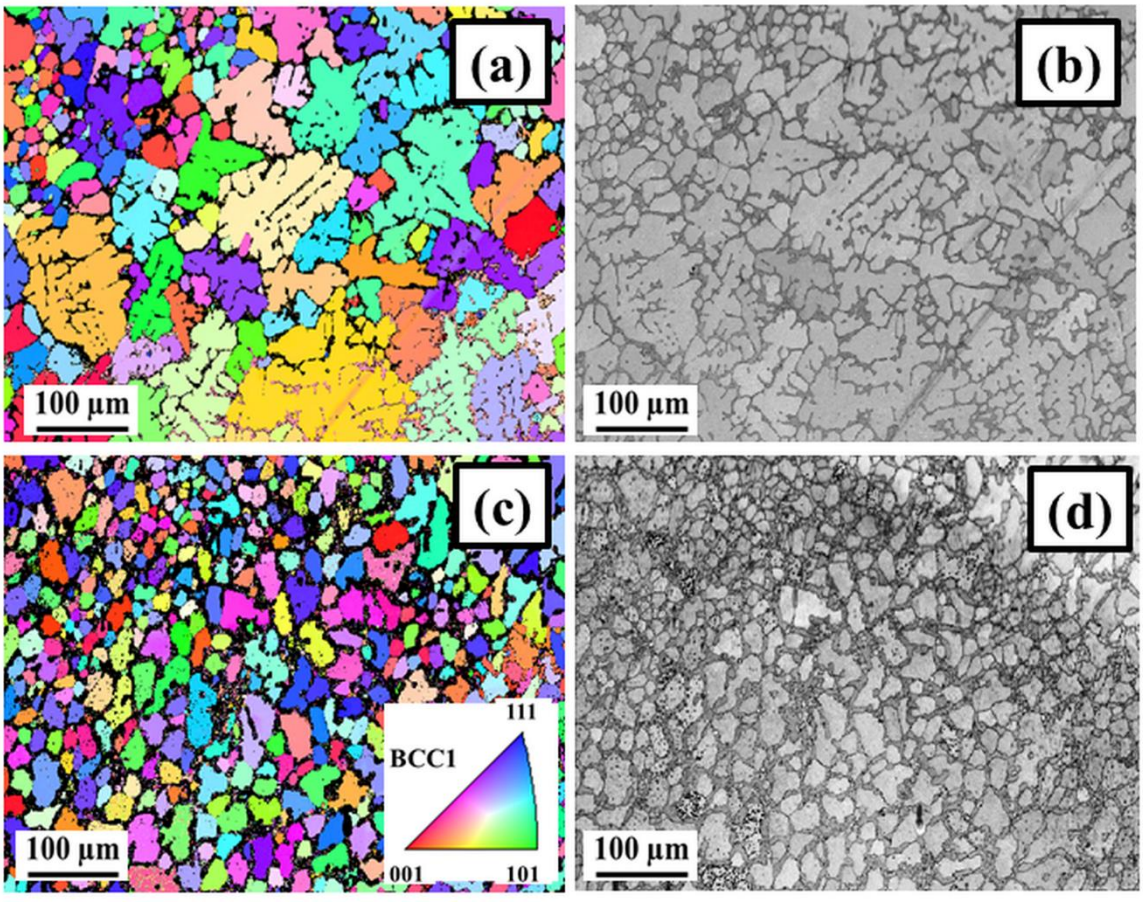

Figure 7.2 EBSD inverse pole figure maps of (a) as-cast CCA and (c) 1100ºC annealed CCA, and (b and d) image quality maps of as-cast and 1100ºC annealed CCA, respectively.

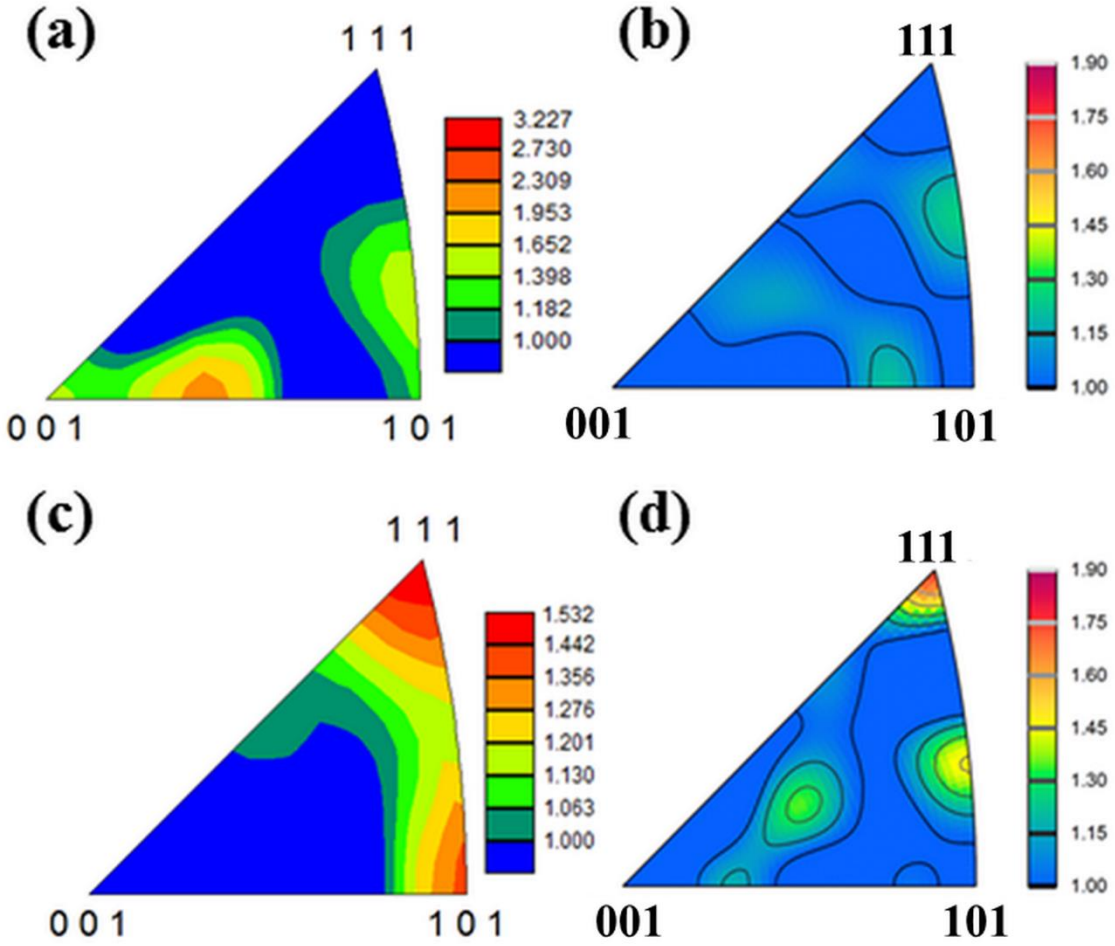

Figure 7.3 Micro- and macro-texture analysis of the as-cast and 1100ºC annealed $Ti_{35}Zr_{35}Nb_{15}Mo_5Fe_5Cr_5$ CCA (a & b) IPFs of as-cast CCA obtained from EBSD and X-ray texture, respectively, (c & d) IPFs of 1100ºC annealed CCA obtained from EBSD and X-ray texture, respectively.

Figure 7.3 shows micro- and macro-texture evolution from the as-cast state to the annealed condition, as evident from the IPFs. After annealing, the grains show a more pronounced crystallographic preferred orientation compared to the as-cast state. Figures 7.3 (a and c) show the EBSD IPFs of the as-cast and annealed CCA, respectively, whereas Figures 7.3 (b and d) exhibit the corresponding X-ray texture IPFs. In the case of annealed

CCA, both micro- and macro-texture IPFs reveal a high intensity of <111>, suggesting that a considerably large number of grains oriented with their surface normal along the <111>. In contrast, the as-cast CCA shows no significant intensity along <111>, suggesting only a small number of grains are oriented along <111>. The enhanced cell adhesion observed in the annealed CCA compared to the as-cast CCA can be attributed to the presence of a large number of <111>-oriented grains, which facilitate better cell adhesion on the surface of the annealed sample.

To analyze the texture components related to texture evolution during annealing, the orientation distribution function (ODF) sections at $\phi_2 = 45^o$, obtained from EBSD and X-ray texture measurements, are shown in Figures 7.4 (a and b) for the as-cast CCA and Figures 7.4 (d and e) for the annealed CCA. A schematic ODF section at $\phi_2 = 45^o$ is included in Figure 7.4 (c) to show the reference positions of standard texture components associated with the BCC structure. In the as-cast CCA sample, the ODF sections do not clearly reveal well-defined standard texture components, aside from the presence of a rotated Cube component within the micro-texture. Additionally, some intensity near the Cube orientation is evident in the macro-texture, while the micro-texture also exhibits slight intensity near the Brass orientation.

In contrast, the macro-texture ODF section of the annealed CCA distinctly reveals the presence of the γ-fiber (<111> || ND) texture component, along with Brass ({110} <111>), Cube, and ε-fiber orientations (Figure 7.4 (e)). The Cube component appears slightly shifted from its ideal orientation. These γ-fiber and Brass components are also evident in the micro-texture analysis. The development of these texture components supports the earlier observation that annealing promotes a greater number of grains oriented along <111>, which

facilitates preferential cell adhesion and contributes to the enhanced biocompatibility of the annealed $Ti_{35}Zr_{35}Nb_{15}Mo_5Fe_5Cr_5$ CCA compared to its as-cast state.

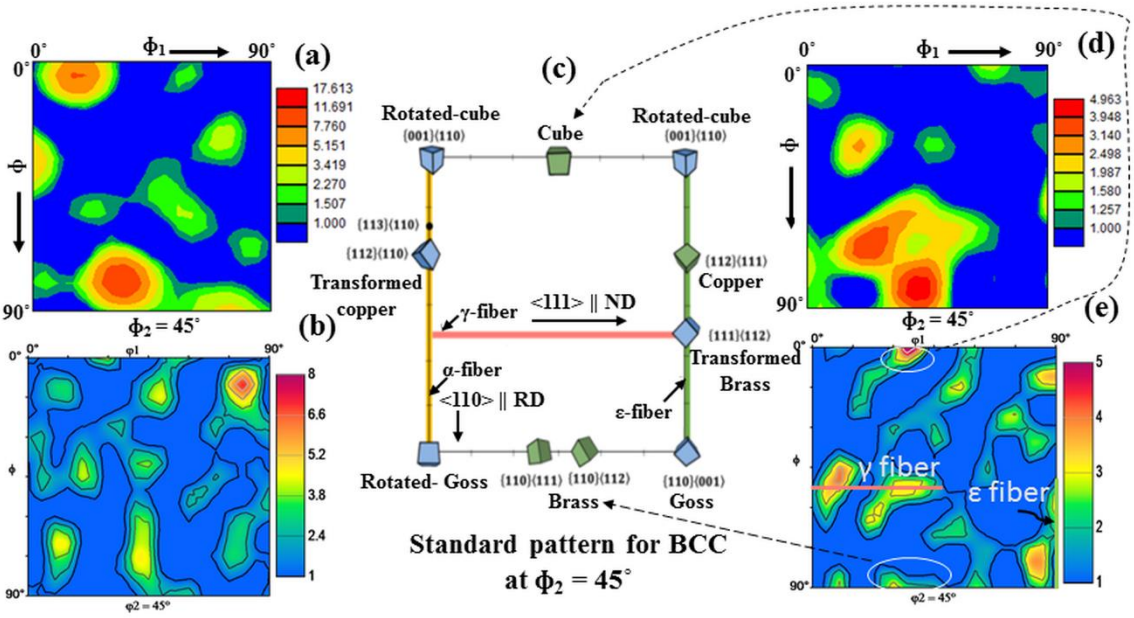

Figure 7.4 Micro- and macro-texture analysis of the as-cast and 1100ºC annealed $Ti_{35}Zr_{35}Nb_{15}Mo_5Fe_5Cr_5$ CCA (a & b) ODF of as-cast CCA at ϕ_2 = 45º obtained from EBSD & X-ray texture, respectively, (c) schematic ODF section showing reference positions of standard texture components at ϕ2 = 45º and (d & e) ODF of 1100ºC annealed CCA at ϕ_2 = 45º obtained from EBSD and X-ray texture, respectively.

7.3 Discussion

Figure 7.5 shows a schematic representation and summary of the mechanism by which crystallographic texture enhances cell adhesion in the annealed CCA sample investigated in this study. As a result of texture evolution, particularly the development of the γ-fiber (<111> || ND), the IPF of the annealed specimen exhibits increased intensity along the [111] direction. This indicates that a considerable number of grains are crystallographically oriented with their [111] direction normal to the IPF map plane, as schematically illustrated in Figure 7.5. In the standard IPF triangle legend, these grains

appear in blue. The schematic also includes two additional orientations to depict the relative crystal orientations of the green and red grains, which correspond to [001] and [101] directions normal to the plane, respectively. During cell culture, a greater number of cells are observed to adhere to the surfaces of the blue grains. This enhanced cell adhesion on grains with a [111] orientation in the normal direction can be attributed to the fact that [111] is the close-packed direction in the BCC structure, which facilitates protein adsorption and thereby promotes enhanced cell adhesion.

The bottom part of the schematic in Figure 7.5 depicts the time-dependent mechanism of cell adhesion. In the initial phase (Stage I), as cells are sown onto the surface of the CCA sample, they undergo sedimentation and settle onto the alloy surface. During this stage, integrins, cell membrane proteins responsible for mediating adhesion, begin to interact with the sample surface. As incubation progresses (Stage II), cell adhesion gradually develops through the formation of integrin-mediated bonds between the cells and the alloy surface [230-231], although the attachment remains relatively weak. Simultaneously, the cells extend protrusions such as filopodia and lamellipodia to increase surface contact. In the later stage of incubation (Stage III), cell spreading occurs through the formation of focal adhesions, where integrins connect to the cytoskeleton, resulting in stronger adhesion. At this stage, cells begin to proliferate and migrate. This progression reflects a maturation process in which the crystallographic orientation of the grains influences the strength of cell adhesion.

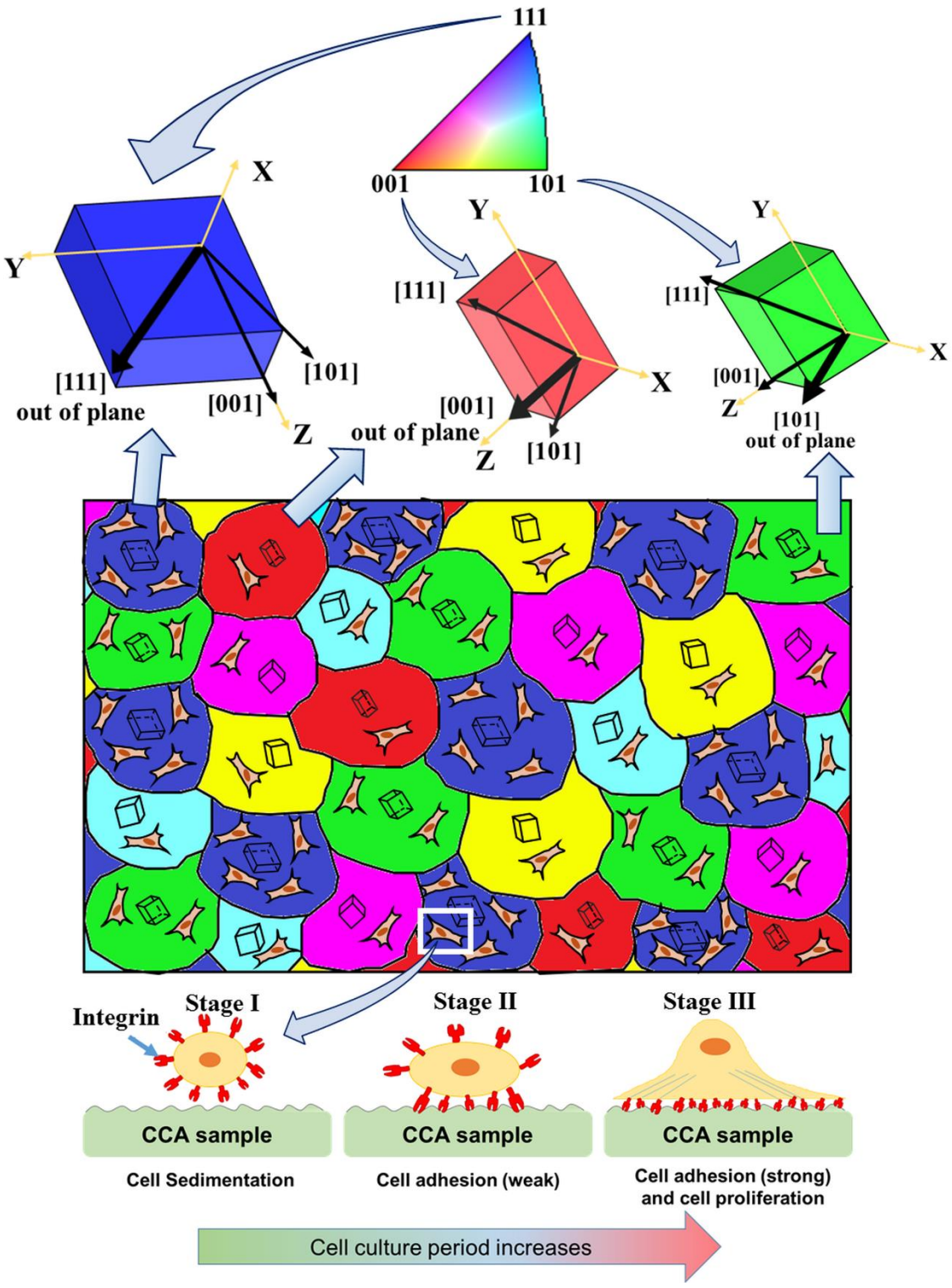

Figure 7.5 Schematic diagram to explain the crystallographic texture dependence of biocompatibility in the present study.

7.4 Summary

This chapter investigates the influence of crystallographic texture on the biocompatibility of the as-cast and annealed $Ti_{35}Zr_{35}Nb_{15}Mo_5Fe_5Cr_5$ CCA. The results of the experimental findings are summarized below.

i. The in-vitro cell culture experiments, including MTT assay and AO/EtBr staining, reveal that the annealed CCA demonstrates enhanced cell viability, adhesion, and proliferation compared to the as-cast CCA.

ii. The SEM images of MG-63 cells on the annealed CCA sample exhibit a greater number of cells with more irregular and polygonal shapes compared to those on the as-cast CCA. This indicates that annealing improves cell adhesion on the CCA surface.

iii. Crystallographic texture significantly influences cell adhesion on the surface of the CCA. In the case of annealed alloy, a larger number of grains are oriented with their <111> direction perpendicular to the surface exposed to cells, while the as-cast alloy contains relatively few grains with this orientation. As the <111> direction represents a close-packed direction, it promotes protein adsorption, thereby enhancing cell adhesion in the annealed specimen with a greater number of <111>-oriented grains.

iv. The higher number of grains oriented normal to the [111] direction in the annealed CCA, as indicated by the prominent intensity at [111] in IPF, suggests the formation of a γ-fiber texture (<111> || ND), along with the presence of Brass, Cube, and ε-fiber components. This distinct evolution of crystallographic texture during annealing is considered a key factor in enhancing cell adhesion and improving the biocompatibility of the annealed CCA.